*mathematics*

MDPI

*Article*

# Efficient Computational Algorithms for Non-Convex Constrained Beamforming in Heterogeneous IoV Backhaul Networks

**Haowen Zheng [1], Zeyu Wang [2], Chun Zhu [1,*], Haifeng Tang [3] and Xinyi Hui [3]**

[1] School of Science, Nanjing University of Posts and Telecommunications, Nanjing 210023, China; b23090028@njupt.edu.cn
[2] School of Communications and Information Engineering, Nanjing University of Posts and Telecommunications, Nanjing 210003, China; 2024010124@njupt.edu.cn
[3] School of Internet of Things, Nanjing University of Posts and Telecommunications, Nanjing 210003, China; b23100215@njupt.edu.cn (H.T.); b24080107@njupt.edu.cn (X.H.)
* Correspondence: zhuchun@njupt.edu.cn

**Abstract**

The rapid expansion of the Internet of Vehicles (IoV) necessitates high-capacity backhaul connectivity, yet the deployment of such networks under strict hardware and power constraints poses significant computational challenges for network optimization. To address this challenge, this paper investigates a joint transmit–receive beamforming optimization problem for narrowband wireless backhaul in IoV networks under constant-modulus constraints. Unlike ideal digital architectures, we focus on cost-effective analog phase shifters, which introduce strictly non-convex constant-modulus constraints, rendering the optimization problem mathematically intractable for standard solvers. Since the resulting problem is highly non-convex, we develop two structured numerical methods: an iterative alternating optimization (AO) method and a joint optimization (JO) method, where AO employs auxiliary WMMSE-guided alternating updates together with constant-modulus projection, while JO jointly updates both beamformers over the constant-modulus feasible set. We compare their achievable sum-rate performance with that of a CDO-based benchmark and analyze their dominant computational costs through representative Big-O complexity expressions. Furthermore, we examine the effect of SVD-based and random feasible initializations on empirical convergence behavior, runtime, and final achievable performance. Simulation results demonstrate that the proposed computational methods significantly improve achievable sum-rate performance compared with the CDO benchmark. Moreover, SVD-based initialization provides a more structured starting point and generally leads to better convergence behavior and lower runtime than random feasible initialization. The empirical timing results further show that AO exhibits faster empirical convergence and requires lower runtime, whereas JO achieves better final sum-rate performance after more iterations.

**Keywords:** IoV backhaul; network resource allocation; computational complexity; non-convex optimization

**MSC:** 46N10; 03D15

check for updates

Academic Editor: Andrea Scozzari

Received: 26 March 2026
Revised: 15 April 2026
Accepted: 15 April 2026
Published: 19 April 2026

**Copyright:** © 2026 by the authors. Licensee MDPI, Basel, Switzerland. This article is an open access article distributed under the terms and conditions of the Creative Commons Attribution (CC BY) license.

## 1. Introduction

The Internet of Vehicles (IoV) is a cornerstone of next-generation intelligent transportation systems. The explosion of sensor data—such as LiDAR streams and high-definition

video—demands not only high-capacity wireless backhaul links between roadside units (RSUs) and edge servers [1,2] but also highly efficient computational frameworks for real-time network resource allocation. In these point-to-point infrastructure links, multiple-input multiple-output (MIMO) beamforming is a primary mechanism for enhancing sum rate. However, as network density increases, the computational burden of optimizing these high-dimensional MIMO systems becomes a critical bottleneck for system performance and reliability [3,4].

Research on beamforming schemes for IoV-based MIMO systems has evolved from basic mathematical models to advanced deep learning, with extensive analysis comparing the structural trade-offs between iterative alternating optimization and global joint optimization frameworks [5–12]. Molisch et al. addressed practical massive-MIMO hybrid beamforming deployment by surveying key architectures and design tradeoffs, providing guidance for implementable hardware-constrained beamforming [5]. Ioushua and Eldar targeted limited-RF-chain hybrid beamforming and proposed a family of analog–digital designs that approach fully digital performance with reduced RF hardware cost [6]. Luo et al. addressed the difficulty of non-convex quadratic beamforming formulations and summarized semidefinite relaxation tools that enable tractable approximations with useful theoretical insights [7]. Ibrahim et al. provided a comprehensive state-of-the-art survey on RIS-aided wireless networks, systematically evaluating joint optimization designs and performance metrics while identifying key research gaps in areas such as computational efficiency, multi-objective optimization, and adaptive configuration for dynamic 6G environments [8]. Arora et al. addressed efficient constant-modulus analog beamforming design and proposed scalable algorithms that improve performance–complexity trade-offs in phase-only beamformer construction [9]. Nguyen et al. targeted the high computational burden of iterative hybrid/CM beamforming and proposed deep-unfolding designs that accelerate inference while maintaining strong spectral-efficiency performance [10]. Luo et al. addressed the spectrum congestion challenges in future networks by investigating the deployment of reconfigurable intelligent surfaces within integrated sensing and communication systems [11]. Griffiths and Jim introduced a foundational generalized sidelobe canceller structure that simplifies linearly constrained adaptive beamforming into a hardware-efficient, unconstrained framework, providing a robust methodology for analyzing steering errors and interference suppression [12].

Recent studies have further expanded the algorithmic landscape of hardware-constrained beamforming and related vehicular communications. In the context of large-scale and high-frequency MIMO systems, representative surveys and overviews have highlighted both the opportunities and implementation challenges of massive-array beamforming and hybrid architectures [13,14]. For vehicular and V2X-related scenarios, recent works have investigated massive-MIMO beamforming, robust secure transmission under CSI uncertainty, and energy-efficient resource allocation for vehicular edge computing networks [15–17]. In addition, constant-envelope design problems have received sustained attention in large-scale MIMO precoding [18,19], while learning-based and manifold-based approaches have also been explored for hybrid beamforming and RIS-related phase optimization [20–22].

Although MIMO beamforming has been widely studied, hardware cost and power consumption are major concerns for large-scale RSU deployment. Traditional fully digital beamforming is too expensive for practical use. Instead, analog beamforming using low-cost phase shifters is more suitable, but it introduces strict constant-modulus constraints. Related unimodular optimization ideas are also relevant to phase-only beamformer design [23]. Currently, relatively limited work has explicitly examined joint transmit–receive

beamforming for such power-limited backhaul systems under stringent constant-modulus hardware constraints [24–28].

Motivated by the above observations, this paper investigates joint beamforming optimization for narrowband IoV backhaul from a computational perspective. Although existing studies have provided important results on hybrid/analog beamforming, constant-modulus design, and related optimization methods, relatively limited attention has been paid to a narrowband IoV backhaul setting in which both the transmit beamformer and the receive combiner are subject to constant-modulus constraints and are optimized jointly under a sum-rate objective. To address this problem, we develop two structured algorithmic frameworks, namely alternating optimization (AO) and joint optimization (JO), for the resulting non-convex constrained formulation. In addition, we study the influence of SVD-based and random feasible initializations on the empirical convergence behavior of the proposed algorithms. Our emphasis is on clarifying the computational trade-offs among convergence behavior, runtime, and achievable performance under different feasible initialization strategies. The main contributions are as follows:

- We formulate and study a joint beamforming scheme for IoV MIMO systems, aiming to maximize achievable sum rate subject to constant-modulus constraints at both the transmitter and receiver.
- We employ both AO and JO methods to handle the joint beamforming optimization problem and analyze the impact of these different approaches on system performance.
- We investigate the empirical convergence behavior of the algorithms under both SVD-based and random feasible initializations, and discuss how the initialization choice affects iteration-level convergence performance and final solution quality.

Throughout the paper, bold uppercase letters such as $\boldsymbol{H}$ and $\boldsymbol{F}$ denote matrices, while bold lowercase letters such as $\boldsymbol{s}$ and $\boldsymbol{w}_t$ denote column vectors. The symbols $(\cdot)^{\mathrm{T}}$ and $(\cdot)^{\mathrm{H}}$ stand for the transpose and the conjugate transpose, respectively. The notation $[\boldsymbol{A}]_{m,t}$ denotes the entry of matrix $\boldsymbol{A}$ at the $m$th row and $t$th column. The operator $\|\cdot\|_2$ denotes the Euclidean norm of a vector, and $\|\cdot\|_F$ denotes the Frobenius norm of a matrix.

The remainder of this paper is organized as follows: Section 2 presents the system model and formulates the sum rate for multiple data streams. Section 3 formulates the joint beamforming optimization problem and provides the AO and JO methods. Section 4 reports simulation settings and numerical results. Section 5 concludes the paper.

## 2. System Model

We consider a narrowband wireless backhaul link within an IoV network, modeled as a high-dimensional resource optimization problem. A roadside access point (AP) with $N_t$ antennas communicates with a stationary edge node with $N_r$ antennas. This architecture, delivering $N_s$ spatial data streams, is characterized by its quasi-static channel state, which provides a stable temporal window for executing advanced computational optimization algorithms. Unlike high-mobility scenarios, the fixed-location geometry allows for a more precise mathematical formulation of the beamforming matrices. However, the deployment of large-scale arrays at both ends significantly increases the computational search space, especially when incorporating strict hardware constraints. To systematically address this, the $N_s$ streams are processed through optimized beamforming operators, as defined by the variables summarized in Table 1. The considered narrowband IoV backhaul architecture is illustrated in Figure 1. In this work, both $F$ and $W$ are implemented by analog phase-shifter networks, so only their phases are adjustable while their entry magnitudes remain constant.

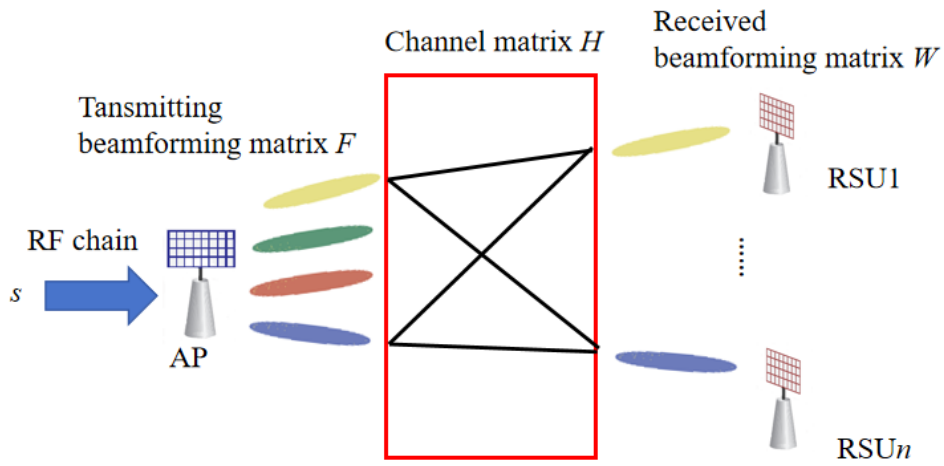



**Figure 1.** System model.

**Table 1.** Main symbols in the system model.

| Symbol | Description | Symbol | Description |
|---|---|---|---|
| $N_t$ | Number of AP transmit antennas | $N_r$ | Number of effective receive antennas |
| $N_s$ | Number of spatial data streams | $L$ | Number of propagation paths |
| $\alpha_\ell$ | Complex gain of the $\ell$th path | $B$ | Bandwidth |
| $\varphi_\ell^{(t)}$ | AoD of the $\ell$th path | $\varphi_\ell^{(r)}$ | AoA of the $\ell$th path |
| $\boldsymbol{H}$ | Narrowband MIMO channel matrix | $\boldsymbol{s}$ | Transmitted symbol vector |
| $s_t$ | The $t$th stream symbol | $\boldsymbol{F}$ | Transmit beamforming matrix |
| $\boldsymbol{W}$ | Receive combining matrix | $\boldsymbol{U}$ | Digital MMSE combiner used in AO |
| $\boldsymbol{V}$ | WMMSE weight matrix used in AO | $\mathrm{SINR}_t$ | SINR of the $t$th stream |
| $t$ | Stream index | $R$ | Achievable sum rate |
| $P$ | Total transmit power | $\sigma^2$ | Noise variance per receive antenna |

In the considered point-to-point backhaul link, the transmitter first maps the $N_s$ data streams to the antenna array through the beamforming matrix $F$, and the receiver then applies the combining matrix $W$ to separate the desired streams from inter-stream interference and noise. Therefore, $F$ and $W$ jointly determine the effective channel seen by each stream and directly affect the achievable sum rate. The underlying narrowband MIMO channel is modeled by a geometric Saleh–Valenzuela model [2,29]. This model captures the small-scale multipath structure of the narrowband channel through a finite number of dominant propagation paths, where each path is characterized by a complex gain $\alpha_\ell$, an angle of departure $\phi_\ell^{(t)}$, and an angle of arrival $\phi_\ell^{(r)}$. Let $L$ denote the number of dominant propagation paths and $\boldsymbol{H} \in \mathbb{C}^{N_r \times N_t}$ be the channel matrix. Under this model,

$$\boldsymbol{H} = \sqrt{\frac{N_t N_r}{L}} \sum_{\ell=1}^{L} \alpha_\ell \, \boldsymbol{a}_r\left(\varphi_\ell^{(r)}\right) \boldsymbol{a}_t^{\mathrm{H}}\left(\varphi_\ell^{(t)}\right). \tag{1}$$

Accordingly, the small-scale fading behavior is reflected by the superposition of these path-dependent complex gains and steering responses. Large-scale effects such as path loss and shadowing are not modeled separately in the present formulation and can be absorbed into the overall channel gain, since the focus of this work is on the beamforming

optimization under a normalized quasi-static backhaul link. For a uniform linear array with antenna spacing $d$ and carrier wavelength $\lambda$, the transmit and receive array response vectors are given by

$$\boldsymbol{a}_t(\varphi) = \frac{1}{\sqrt{N_t}}\left[1, e^{j2\pi\frac{d}{\lambda}\sin\varphi}, \ldots, e^{j2\pi\frac{d}{\lambda}(N_t-1)\sin\varphi}\right]^{\mathrm{T}}, \tag{2}$$

$$\boldsymbol{a}_r(\varphi) = \frac{1}{\sqrt{N_r}}\left[1, e^{j2\pi\frac{d}{\lambda}\sin\varphi}, \ldots, e^{j2\pi\frac{d}{\lambda}(N_r-1)\sin\varphi}\right]^{\mathrm{T}}. \tag{3}$$

Let $\boldsymbol{s} = [s_1, \ldots, s_{N_s}]^{\mathrm{T}} \in \mathbb{C}^{N_s}$ denote the transmitted data streams, normalized as $\mathbb{E}[\boldsymbol{s}\boldsymbol{s}^{\mathrm{H}}] = \boldsymbol{I}_{N_s}$. The transmit beamformer is $\boldsymbol{F} = [\boldsymbol{f}_1, \ldots, \boldsymbol{f}_{N_s}]$, and the transmitted signal is $\boldsymbol{x} = \boldsymbol{F}\boldsymbol{s}$. Therefore, the average transmit power satisfies

$$P = \mathbb{E}\left[\|\boldsymbol{x}\|_2^2\right] = \|\boldsymbol{F}\|_F^2. \tag{4}$$

The received signal at the edge node is given by

$$\boldsymbol{y} = \boldsymbol{H}\boldsymbol{F}\boldsymbol{s} + \boldsymbol{n}, \tag{5}$$

where $\boldsymbol{n} \sim \mathcal{CN}(\boldsymbol{0}, \sigma^2\boldsymbol{I}_{N_r})$ denotes spatially white receiver noise. The receiver applies linear combining $\boldsymbol{W} = [\boldsymbol{w}_1, \ldots, \boldsymbol{w}_{N_s}]$ to estimate the transmitted streams. After combining, the stream estimates are

$$\hat{\boldsymbol{s}} = \boldsymbol{W}^{\mathrm{H}}\boldsymbol{y} = \boldsymbol{W}^{\mathrm{H}}\boldsymbol{H}\boldsymbol{F}\boldsymbol{s} + \boldsymbol{W}^{\mathrm{H}}\boldsymbol{n}. \tag{6}$$

To evaluate per-stream performance, we focus on the $t$th stream output $\hat{s}_t$. By expanding Equation (6) along the $t$th combiner $\boldsymbol{w}_t$, the output naturally decomposes into three parts: the desired signal of stream $t$, the inter-stream interference contributed by all $k \neq t$, and the filtered noise term. Specifically,

$$\hat{s}_t = \boldsymbol{w}_t^{\mathrm{H}}\boldsymbol{H}\boldsymbol{f}_t s_t + \sum_{k\neq t}\boldsymbol{w}_t^{\mathrm{H}}\boldsymbol{H}\boldsymbol{f}_k s_k + \boldsymbol{w}_t^{\mathrm{H}}\boldsymbol{n}. \tag{7}$$

The desired signal is the $t$th stream after passing through its matched beamforming pair $\boldsymbol{w}_t$ and $\boldsymbol{f}_t$. Moreover, the interference arises from all other streams $\boldsymbol{f}_k$ ($k \neq t$) that are also captured by the combiner $\boldsymbol{w}_t$. Furthermore, the effective noise is the antenna noise scaled by the norm of the receive combiner $\boldsymbol{w}_t$.

$$\mathrm{SINR}_t = \frac{\left|\boldsymbol{w}_t^{\mathrm{H}}\boldsymbol{H}\boldsymbol{f}_t\right|^2}{\sum_{k\neq t}\left|\boldsymbol{w}_t^{\mathrm{H}}\boldsymbol{H}\boldsymbol{f}_k\right|^2 + \sigma^2\|\boldsymbol{w}_t\|_2^2}. \tag{8}$$

The rate of each individual stream is determined by its corresponding signal-to-interference-plus-noise ratio (SINR). Accordingly, the achievable sum rate of the considered system can be expressed as

$$R(\boldsymbol{F}, \boldsymbol{W}) = B\sum_{t=1}^{N_s}\log_2\left(1 + \mathrm{SINR}_t\right). \tag{9}$$

Since this performance metric is jointly determined by the transmit beamformer $\boldsymbol{F}$ and the receive combiner $\boldsymbol{W}$ through the effective SINRs of all streams; the subsequent beamforming design problem aims to optimize $\boldsymbol{F}$ and $\boldsymbol{W}$ so as to maximize $R(\boldsymbol{F}, \boldsymbol{W})$ under the constant-modulus constraints.

## 3. Problem Formulation

To solve the joint beamforming problem, we consider two different optimization strategies. The first one is AO, which alternately updates the transmit and receive beamformers by solving simpler subproblems while keeping the other side fixed. The second one is JO, which treats the transmit and receive beamformers as a coupled variable pair and updates them jointly through projected gradient iterations. Therefore, AO emphasizes stepwise decoupling and stable local improvement, whereas JO emphasizes direct joint search over the original non-convex feasible set.

Primarily, our goal is to jointly design $F$ and $W$ to maximize $R(F, W)$, which can be described as

$$\max_{\boldsymbol{F},\boldsymbol{W}} \; R(\boldsymbol{F}, \boldsymbol{W}) \tag{10}$$

In power-limited IoV MIMO systems, analog phase shifters and power-efficient RF components often impose constant-modulus constraints. We therefore consider constant-modulus constraints on the transmit beamformer entries together with a total power constraint

$$\|\boldsymbol{F}\|_F^2 = P, \qquad \left|[\boldsymbol{F}]_{m,t}\right| = \sqrt{\tfrac{P}{N_t N_s}}. \; \forall m, t \tag{11}$$

At the receiver, we consider the constant-modulus constraint with normalized amplitude, which can be expressed as

$$|[W]_{m,t}| = \frac{1}{\sqrt{N_r}}, \quad \forall m, t \tag{12}$$

Considering the power-limited nature of IoV MIMO systems and the hardware constraints imposed by analog phase shifters, we formulate the joint sum rate maximization problem subject to transceiver constant-modulus constraints as

$$\max_{\boldsymbol{F},\boldsymbol{W}} \quad R(\boldsymbol{F}, \boldsymbol{W}) \tag{13a}$$

$$\text{s.t.} \quad \left|[\boldsymbol{F}]_{m,t}\right| = \sqrt{\frac{P}{N_t N_s}}, \quad \forall m, t, \tag{13b}$$

$$\left|[\boldsymbol{W}]_{m,t}\right| = \frac{1}{\sqrt{N_r}}, \quad \forall m, t \tag{13c}$$

The optimization problem in Equation (13) is non-convex in both the objective function and the feasible set. Specifically, the objective $R(F, W)$ is not jointly concave in $F$ and $W$, because each $\mathrm{SINR}_t$ in Equation (8) is a ratio of coupled quadratic terms involving the bilinear form $w_t^H H f_k$, and the desired-signal and inter-stream interference terms are jointly coupled across all streams. In addition, the constraints are also non-convex. The constant-modulus equalities $|[F]_{m,t}| = \sqrt{P/(N_t N_s)}$ and $|[W]_{m,t}| = 1/\sqrt{N_r}$ define non-convex feasible sets, since a convex combination of two feasible phase-only points does not, in general, preserve the same modulus. Therefore, Equation (13) is intrinsically non-convex, which motivates the AO and JO algorithms developed below.

### *3.1. AO Method*

AO is introduced as a computationally light alternating heuristic for the hardware-constrained problem. Unlike JO, the AO scheme does not directly solve each block of the original constant-modulus problem. Instead, for a given transmit beamformer, we first compute an auxiliary digital MMSE combiner and the associated WMMSE weight matrix, and then use them to construct a tractable surrogate update for the transmit side. The actual hardware-feasible receive combiner is not the digital MMSE combiner itself, but

its phase-projected constant-modulus version. Therefore, the auxiliary variables are used only to guide the alternating updates, while the final beamforming matrices remain the constant-modulus pair $(\boldsymbol{F}, \boldsymbol{W})$. Since the receive-side and transmit-side projections break the exact WMMSE equivalence of the unconstrained setting, the AO scheme should be interpreted as a WMMSE-inspired heuristic algorithm. Accordingly, no rigorous stationary-point convergence guarantee is claimed for AO, and only empirical convergence behavior is reported in Section 4.

For a fixed transmit beamformer $\boldsymbol{F}$, define the received covariance matrix as

$$\boldsymbol{R}_{yy} = \boldsymbol{H}\boldsymbol{F}\boldsymbol{F}^{\mathrm{H}}\boldsymbol{H}^{\mathrm{H}} + \sigma^2 \boldsymbol{I}_{N_r}. \tag{14}$$

The corresponding auxiliary digital MMSE combiner is

$$\boldsymbol{U} = \boldsymbol{R}_{yy}^{-1}\boldsymbol{H}\boldsymbol{F}. \tag{15}$$

To obtain a hardware-feasible analog receive combiner, we project $\boldsymbol{U}$ onto the constant-modulus set:

$$[\boldsymbol{W}]_{m,t} = \frac{1}{\sqrt{N_r}} \exp\big(j \angle([\boldsymbol{U}]_{m,t})\big), \qquad \forall m, t. \tag{16}$$

Hence, $\boldsymbol{U}$ is only an auxiliary digital variable, whereas $\boldsymbol{W}$ is the actual analog combiner used to evaluate the achievable sum rate.

Using $\boldsymbol{U}$, the WMMSE error matrix is written as

$$\boldsymbol{E} = \boldsymbol{I}_{N_s} - \boldsymbol{F}^{\mathrm{H}}\boldsymbol{H}^{\mathrm{H}}\boldsymbol{U} - \boldsymbol{U}^{\mathrm{H}}\boldsymbol{H}\boldsymbol{F} + \boldsymbol{U}^{\mathrm{H}}\Big(\boldsymbol{H}\boldsymbol{F}\boldsymbol{F}^{\mathrm{H}}\boldsymbol{H}^{\mathrm{H}} + \sigma^2 \boldsymbol{I}_{N_r}\Big)\boldsymbol{U}. \tag{17}$$

We then define the WMMSE weight matrix as

$$\boldsymbol{V} = \big(\boldsymbol{E} + \delta \boldsymbol{I}_{N_s}\big)^{-1}, \tag{18}$$

where a small $\delta > 0$ is used for numerical stability. For fixed $\boldsymbol{U}$ and $\boldsymbol{V}$, an unconstrained transmit-side surrogate update is

$$\boldsymbol{F}_{\mathrm{raw}} = \Big(\boldsymbol{H}^{\mathrm{H}}\boldsymbol{U}\boldsymbol{V}\boldsymbol{U}^{\mathrm{H}}\boldsymbol{H} + \epsilon \boldsymbol{I}_{N_t}\Big)^{-1}\boldsymbol{H}^{\mathrm{H}}\boldsymbol{U}\boldsymbol{V}, \tag{19}$$

where $\epsilon > 0$ is a small regularization parameter. Finally, the transmit beamformer is projected onto the constant-modulus feasible set:

$$[\boldsymbol{F}]_{m,t} = \sqrt{\frac{P}{N_t N_s}} \exp\big(j \angle([\boldsymbol{F}_{\mathrm{raw}}]_{m,t})\big), \qquad \forall m, t. \tag{20}$$

It is worth emphasizing that the AO method operates through auxiliary digital updates followed by constant-modulus projections. Therefore, unlike the standard unconstrained WMMSE framework, the resulting AO iteration is not an exact block-coordinate optimization procedure for the original constant-modulus problem. In particular, the present manuscript does not claim strict monotonicity of the objective sequence or a formal proof of convergence to a stationary point. The role of AO in this work is to provide a practical low-complexity heuristic baseline for comparison with JO. The detailed steps of the AO procedure are summarized in Algorithm 1.

**Algorithm 1** AO Method (WMMSE-Inspired Alternating Heuristic)

**Require:** Channel $\boldsymbol{H}$, noise variance $\sigma^2$, power $P$, number of streams $N_s$, maximum iterations $I_{\max}$, tolerance $\varepsilon$, small constants $\delta, \epsilon$
**Ensure:** $\boldsymbol{F}^\star$, $\boldsymbol{W}^\star$, sum rate $R^\star$
Compute SVD $\boldsymbol{H} = \boldsymbol{U}_H \boldsymbol{\Sigma} \boldsymbol{V}_H^{\mathrm{H}}$
Initialize transmit beamformer by SVD-phase projection: $\boldsymbol{F}^{(0)} = \sqrt{\frac{P}{N_t N_s}} \exp\big(j \angle(\boldsymbol{V}_H(:, 1:N_s))\big)$
Compute $\boldsymbol{R}_{yy}^{(0)} = \boldsymbol{H}\boldsymbol{F}^{(0)}(\boldsymbol{F}^{(0)})^{\mathrm{H}}\boldsymbol{H}^{\mathrm{H}} + \sigma^2 \boldsymbol{I}_{N_r}$
Compute the auxiliary digital combiner $\boldsymbol{U}^{(0)} = (\boldsymbol{R}_{yy}^{(0)})^{-1}\boldsymbol{H}\boldsymbol{F}^{(0)}$
Obtain the feasible analog combiner $\boldsymbol{W}^{(0)}$ by (16)
Compute $R^{(0)} = R(\boldsymbol{F}^{(0)}, \boldsymbol{W}^{(0)})$
**for** $i = 0, 1, \ldots, I_{\max} - 1$ **do**
  Compute $\boldsymbol{R}_{yy}^{(i)} = \boldsymbol{H}\boldsymbol{F}^{(i)}(\boldsymbol{F}^{(i)})^{\mathrm{H}}\boldsymbol{H}^{\mathrm{H}} + \sigma^2 \boldsymbol{I}_{N_r}$
  Compute the auxiliary digital combiner $\widetilde{\boldsymbol{U}} = (\boldsymbol{R}_{yy}^{(i)})^{-1}\boldsymbol{H}\boldsymbol{F}^{(i)}$
  Form $\widetilde{\boldsymbol{E}}$ using (17) with $\boldsymbol{F} = \boldsymbol{F}^{(i)}$ and $\boldsymbol{U} = \widetilde{\boldsymbol{U}}$
  Set $\widetilde{\boldsymbol{V}} = \big(\widetilde{\boldsymbol{E}} + \delta \boldsymbol{I}_{N_s}\big)^{-1}$
  Compute $\boldsymbol{F}_{\mathrm{raw}}$ from (19) with $\boldsymbol{U} = \widetilde{\boldsymbol{U}}$ and $\boldsymbol{V} = \widetilde{\boldsymbol{V}}$
  Project $\boldsymbol{F}_{\mathrm{raw}}$ by (20) to obtain $\boldsymbol{F}^{(i+1)}$
  Compute $\boldsymbol{R}_{yy}^{(i+1)} = \boldsymbol{H}\boldsymbol{F}^{(i+1)}(\boldsymbol{F}^{(i+1)})^{\mathrm{H}}\boldsymbol{H}^{\mathrm{H}} + \sigma^2 \boldsymbol{I}_{N_r}$
  Compute the auxiliary digital combiner $\boldsymbol{U}^{(i+1)} = (\boldsymbol{R}_{yy}^{(i+1)})^{-1}\boldsymbol{H}\boldsymbol{F}^{(i+1)}$
  Obtain the feasible analog combiner $\boldsymbol{W}^{(i+1)}$ by (16)
  Compute $R^{(i+1)} = R(\boldsymbol{F}^{(i+1)}, \boldsymbol{W}^{(i+1)})$
  **if** $\big|R^{(i+1)} - R^{(i)}\big| / \max\{1, R^{(i)}\} \le \varepsilon$ **then**
    **break**
  **end if**
**end for**
Output $\boldsymbol{F}^\star = \boldsymbol{F}^{(i+1)}$, $\boldsymbol{W}^\star = \boldsymbol{W}^{(i+1)}$, $R^\star = R^{(i+1)}$

### *3.2. JO Method*

JO follows a different philosophy: instead of splitting the variables into alternating subproblems, it directly optimizes the original objective under the joint constant-modulus constraints. We rewrite the problem as minimizing the negative sum rate:

$$\min_{\boldsymbol{F}, \boldsymbol{W}} \quad -R(\boldsymbol{F}, \boldsymbol{W}) \tag{21a}$$

$$\text{s.t.} \quad (11) \text{ and } (12). \tag{21b}$$

A practical approach is to apply gradient-based updates and then project the updated variables back onto the constant-modulus sets. In the revised manuscript, the JO method is implemented with an Armijo backtracking line search, so that each iteration consists of gradient evaluation, a joint update of $\boldsymbol{F}$ and $\boldsymbol{W}$, and element-wise projection onto the constant-modulus feasible sets. Since the problem is non-convex, the final solution may depend on the initialization. Therefore, JO is combined with multi-start, and the best solution across different initial points is selected as the final output [30].

To explicitly state the gradient expressions used in JO, let $\boldsymbol{e}_t \in \mathbb{R}^{N_s}$ denote the $t$th canonical basis vector and define

$$\boldsymbol{J}_t = \boldsymbol{I}_{N_s} - \boldsymbol{e}_t \boldsymbol{e}_t^{\mathsf{T}}. \tag{22}$$

Note that $\boldsymbol{J}_t$ is real and symmetric, i.e., $\boldsymbol{J}_t^{\mathsf{T}} = \boldsymbol{J}_t$. For the $t$th stream, define

$$\boldsymbol{Q}_t = \boldsymbol{H}^{\mathsf{H}} \boldsymbol{w}_t \boldsymbol{w}_t^{\mathsf{H}} \boldsymbol{H}, \tag{23}$$

where $\boldsymbol{w}_t$ is the $t$th column of $\boldsymbol{W}$. Then the $t$th stream rate can be written as

$$R_t(\boldsymbol{F}, \boldsymbol{W}) = B \log_2\left(\frac{u_t}{v_t}\right), \tag{24}$$

with

$$u_t = \mathrm{Tr}(\boldsymbol{F}^{\mathsf{H}} \boldsymbol{Q}_t \boldsymbol{F}) + \sigma^2 \|\boldsymbol{w}_t\|_2^2, \qquad v_t = \mathrm{Tr}(\boldsymbol{F}^{\mathsf{H}} \boldsymbol{Q}_t \boldsymbol{F} \boldsymbol{J}_t) + \sigma^2 \|\boldsymbol{w}_t\|_2^2. \tag{25}$$

Hence,

$$R(\boldsymbol{F}, \boldsymbol{W}) = \sum_{t=1}^{N_s} R_t(\boldsymbol{F}, \boldsymbol{W}). \tag{26}$$

Using Wirtinger calculus, the derivative of $R(\boldsymbol{F}, \boldsymbol{W})$ with respect to $\boldsymbol{F}^*$ is

$$\frac{\partial R}{\partial \boldsymbol{F}^*} = \frac{B}{\ln 2} \sum_{t=1}^{N_s} \left( \frac{\boldsymbol{Q}_t \boldsymbol{F}}{u_t} - \frac{\boldsymbol{Q}_t \boldsymbol{F} \boldsymbol{J}_t}{v_t} \right). \tag{27}$$

Therefore,

$$\frac{\partial(-R)}{\partial \boldsymbol{F}^*} = -\frac{\partial R}{\partial \boldsymbol{F}^*}. \tag{28}$$

For the receive side, define

$$\boldsymbol{C} = \boldsymbol{H}\boldsymbol{F}\boldsymbol{F}^{\mathsf{H}}\boldsymbol{H}^{\mathsf{H}} + \sigma^2 \boldsymbol{I}_{N_r}, \qquad \boldsymbol{D}_t = \boldsymbol{H}\boldsymbol{F}\boldsymbol{J}_t\boldsymbol{F}^{\mathsf{H}}\boldsymbol{H}^{\mathsf{H}} + \sigma^2 \boldsymbol{I}_{N_r}. \tag{29}$$

Then $u_t = \boldsymbol{w}_t^{\mathsf{H}} \boldsymbol{C} \boldsymbol{w}_t$ and $v_t = \boldsymbol{w}_t^{\mathsf{H}} \boldsymbol{D}_t \boldsymbol{w}_t$, and the derivative of $R(\boldsymbol{F}, \boldsymbol{W})$ with respect to $\boldsymbol{w}_t^*$ is

$$\frac{\partial R}{\partial \boldsymbol{w}_t^*} = \frac{B}{\ln 2} \left( \frac{\boldsymbol{C}\boldsymbol{w}_t}{u_t} - \frac{\boldsymbol{D}_t \boldsymbol{w}_t}{v_t} \right). \tag{30}$$

By stacking the columnwise derivatives, we obtain

$$\frac{\partial R}{\partial \boldsymbol{W}^*} = \left[ \frac{\partial R}{\partial \boldsymbol{w}_1^*}, \frac{\partial R}{\partial \boldsymbol{w}_2^*}, \ldots, \frac{\partial R}{\partial \boldsymbol{w}_{N_s}^*} \right]. \tag{31}$$

Therefore,

$$\frac{\partial(-R)}{\partial \boldsymbol{W}^*} = -\frac{\partial R}{\partial \boldsymbol{W}^*}. \tag{32}$$

The JO update then takes the form of a projected gradient step:

$$\boldsymbol{F}^{(i+1)} = \Pi_{\mathcal{F}}\left( \boldsymbol{F}^{(i)} - \mu_i \frac{\partial(-R)}{\partial \boldsymbol{F}^*} \right), \tag{33}$$

$$\boldsymbol{W}^{(i+1)} = \Pi_{\mathcal{W}}\left( \boldsymbol{W}^{(i)} - \mu_i \frac{\partial(-R)}{\partial \boldsymbol{W}^*} \right), \tag{34}$$

where $\mu_i$ is chosen by Armijo backtracking line search, and $\Pi_{\mathcal{F}}(\cdot)$ and $\Pi_{\mathcal{W}}(\cdot)$ denote the element-wise constant-modulus projections:

$$[\Pi_{\mathcal{F}}(\boldsymbol{X})]_{m,t} = \sqrt{\frac{P}{N_t N_s}} \exp\big(j\angle([\boldsymbol{X}]_{m,t})\big), \qquad [\Pi_{\mathcal{W}}(\boldsymbol{Y})]_{m,t} = \frac{1}{\sqrt{N_r}} \exp\big(j\angle([\boldsymbol{Y}]_{m,t})\big). \tag{35}$$

It is also worth noting that, for each fixed SNR value and each fixed initialization in the inner loop, the JO updates constitute a line-search projected gradient scheme over the

compact constant-modulus feasible set. Since $\sigma^2 > 0$, all SINR denominators are strictly positive, and therefore the objective function $-R(\boldsymbol{F}, \boldsymbol{W})$ is smooth on the feasible set. Moreover, the constant-modulus projection in Equation (35) can be interpreted as a retraction on this feasible set. Therefore, by standard convergence results for projected/Riemannian gradient methods with line search [27,28], the corresponding objective sequence is non-increasing, and every accumulation point of the generated inner iterate sequence is a first-order stationary point of Equation (21). The detailed steps of the JO procedure are summarized in Algorithm 2.

**Algorithm 2** JO Method (Projected Gradient with Armijo Line Search and Multi-Start)

**Require:** Channel $\boldsymbol{H}$, noise variance $\sigma^2$, nominal transmit-side SNR set $\{\gamma_{\mathrm{dB}}\}$, maximum iterations $I_{\max}$, number of starts $N_{\mathrm{start}}$, Armijo parameters
**Ensure:** For each SNR: $\boldsymbol{F}^\star$, $\boldsymbol{W}^\star$, sum rate $R^\star$
Compute SVD $\boldsymbol{H} = \boldsymbol{U}_H \boldsymbol{\Sigma} \boldsymbol{V}_H^{\mathrm{H}}$
Initialize warm start as empty
**for** each $\gamma_{\mathrm{dB}}$ **do**
  Set $\gamma = 10^{\gamma_{\mathrm{dB}}/10}$ and $P = \gamma\sigma^2$
  Build SVD-phase feasible initialization: $\boldsymbol{F}_{\mathrm{svd}} = \sqrt{\frac{P}{N_t N_s}} \exp\big(j\angle(\boldsymbol{V}_H(:, 1 : N_s))\big)$, $\boldsymbol{W}_{\mathrm{svd}} = \frac{1}{\sqrt{N_r}} \exp\big(j\angle(\boldsymbol{U}_H(:, 1 : N_s))\big)$
  Set best value $R^\star = -\infty$
  **for** $q = 1, 2, \ldots, N_{\mathrm{start}}$ **do**
    If $q = 1$, use warm start if available; otherwise use $(\boldsymbol{F}_{\mathrm{svd}}, \boldsymbol{W}_{\mathrm{svd}})$
    If $q \geq 2$, generate random feasible phases satisfying the constant-modulus constraints
    **for** $i = 0, 1, \ldots, I_{\max} - 1$ **do**
      Compute $\frac{\partial(-R)}{\partial \boldsymbol{F}^*}$ and $\frac{\partial(-R)}{\partial \boldsymbol{W}^*}$ using (27), (28), (30), and (32)
      Choose the step size $\mu_i$ by Armijo backtracking line search
      Update $\boldsymbol{F}$ and $\boldsymbol{W}$ using (33) and (34)
    **end for**
    Compute achieved $R(\boldsymbol{F}, \boldsymbol{W})$ and update the best solution if larger than $R^\star$
  **end for**
  Update warm start with the best solution at this SNR
**end for**

At the end of this section, we emphasize the role of feasible initialization. Here, the warm start means that the best solution obtained at the previous SNR is reused as the first initialization for the next SNR, which improves continuity in the SNR sweep and reduces unnecessary research. Since the problem is non-convex and the feasible set is highly constrained by constant modulus, different initial points can lead to different stationary solutions and different convergence speeds. Therefore, we adopt SVD-phase initialization as a practical default because it provides a structured and usually strong starting point, and we additionally compare SVD-phase versus random feasible initializations in the convergence analysis to quantify the convergence speed and stability advantage. In addition, the phase-shifter adjustment in both AO and JO is implemented through simple constant-modulus projection, while the main extra computational burden mainly comes from the SVD-based initialization and the multi-start strategy adopted by JO. Hence, similar iteration counts should not be directly interpreted as similar overall computational cost.

### *3.3. Computational Complexity Analysis*

We next provide a representative Big-$O$ analysis for one problem instance, i.e., one channel realization at one SNR point, in order to compare the computational behaviors of AO and JO. Here we retain only the dominant operations, such as matrix multiplications, matrix inversions or linear-system solves, singular value decomposition, gradient-related

evaluations, and constant-modulus projection, while lower-order terms, constant factors, and implementation-dependent overhead are omitted. Let $I_{\mathrm{AO}}$ and $I_{\mathrm{JO}}$ denote the iteration numbers of AO and JO, respectively. When repeated restarts are used in JO, their number is denoted by $N_{\mathrm{start}}$.

First, both algorithms can employ the same SVD-phase feasible initialization. For the channel matrix $H \in \mathbb{C}^{N_r \times N_t}$, the one-time economy-size SVD incurs the cost

$$\mathcal{C}_{\mathrm{SVD}} = O\Big(\min\{N_r N_t^2,\ N_t N_r^2\}\Big). \tag{36}$$

This term is paid once for each problem instance and is therefore more naturally viewed as a preprocessing cost.

For AO, each outer iteration consists of alternating updates of the receiver-side and transmitter-side beamformers, together with the corresponding constant-modulus projection steps. At a representative level, the dominant computations arise from forming effective covariance or Gram-type matrices, carrying out matrix multiplications, and solving the associated linear-algebra subproblems. Therefore, a representative upper bound for the per-iteration complexity of AO can be written as

$$\mathcal{C}_{\mathrm{AO,iter}} = O\Big(N_r^3 + N_t^3 + N_r^2 N_s + N_t^2 N_s + N_r N_t N_s\Big). \tag{37}$$

Accordingly, the total complexity of AO may be expressed as

$$\mathcal{C}_{\mathrm{AO}} = O\Big(\min\{N_r N_t^2,\ N_t N_r^2\} + I_{\mathrm{AO}}\Big(N_r^3 + N_t^3 + N_r^2 N_s + N_t^2 N_s + N_r N_t N_s\Big)\Big). \tag{38}$$

In the common regime $N_s \ll \min\{N_t, N_r\}$, the AO complexity can be further summarized as

$$\mathcal{C}_{\mathrm{AO}} \approx O\Big(\mathcal{C}_{\mathrm{SVD}} + I_{\mathrm{AO}}(N_r^3 + N_t^3)\Big). \tag{39}$$

This expression should be interpreted as a scaling law rather than an exact runtime model.

For JO, each iteration jointly updates the transmit and receive beamformers according to the adopted optimization strategy, followed by feasibility enforcement on the constant-modulus constraints. In a representative implementation, the dominant arithmetic burden comes from forming effective products involving $H$, $F$, and $W$, together with the corresponding objective-related or search-direction-related computations. Since the element-wise constant-modulus projection is only linear in the number of entries, it is usually not the dominant cost. A representative per-iteration complexity estimate for JO is

$$\mathcal{C}_{\mathrm{JO,iter}} = O\Big(N_r N_t N_s + (N_r + N_t) N_s^2\Big). \tag{40}$$

If multiple restarts or multiple candidate initializations are adopted, the total JO complexity scales linearly with the corresponding number of trials. Hence, a representative total complexity expression is

$$\mathcal{C}_{\mathrm{JO}} = O\Big(\min\{N_r N_t^2,\ N_t N_r^2\} + N_{\mathrm{start}} I_{\mathrm{JO}}\Big(N_r N_t N_s + (N_r + N_t) N_s^2\Big)\Big), \tag{41}$$

where one may simply set $N_{\mathrm{start}} = 1$ when no restart mechanism is used.

The above expressions indicate that AO and JO exhibit different computational characteristics at the asymptotic level. More importantly, these complexity expressions should be understood as theoretical scaling descriptions rather than exact predictors of measured wall-clock time. In practice, the observed runtime is also affected by factors such as initialization quality, restart policy, convergence tolerance, and implementation overhead.

Therefore, the computational comparison between AO and JO should distinguish between asymptotic complexity and empirical runtime, and the latter will be further examined in the simulation results.

## 4. Simulation Results and Analysis

In this section, we evaluate the proposed computational frameworks under a representative narrowband IoV backhaul scenario with constant-modulus transceiver constraints. Simulation parameters are summarized in Table 2.

**Table 2.** Simulation parameters.

| Symbol | Value | Symbol | Value |
|---|---|---|---|
| $N_t$ | 64 | $N_r$ | 16 |
| $N_s$ | 4 | $\sigma^2$ | 0.01 |
| $L$ | 10 | $B$ | 1 |
| $\gamma_{\mathrm{dB}}$ | 0:5:40 dB | $d/\lambda$ | 0.5 |

Specifically, $\gamma_{dB}$ denotes the nominal SNR defined by $\gamma = P/\sigma^2$. To ensure a consistent physical interpretation, the channel matrix $\mathbf{H}$ is normalized such that $\mathbb{E}[\|\mathbf{H}\|_F^2] = N_r N_t$. Under this normalization, $\gamma$ effectively represents the average receive SNR per antenna, as the channel does not introduce additional bulk path loss in the statistical sense. The actual receive-side performance is then evaluated by the post-combining SINR in Equation (8). For each channel realization, the narrowband MIMO channel is generated according to the geometric Saleh–Valenzuela model with $L$ dominant paths, ensuring that the reported results account for the corresponding multipath small-scale fading.

All simulations are implemented in MATLAB (R2025B). No external dataset is used in this work. Instead, all numerical results are obtained from synthetically generated narrowband MIMO channel realizations according to the geometric Saleh–Valenzuela model. For each SNR point, the results in Figure 2 are averaged over 100 independent channel realizations. The boxplot in Figure 3 is also obtained from 100 independent Monte Carlo trials.

We compare three schemes, namely, the proposed joint optimization (JO) method, the alternating optimization (AO) method, and the CDO-based benchmark. The CDO-based benchmark is adopted as the main reference because it provides a direct and fair comparison under the same constant-modulus transceiver constraints as the proposed methods. In particular, CDO operates on the same hardware-feasible design space and does not rely on relaxed unconstrained digital beamforming assumptions. Therefore, compared with benchmarks based on mismatched feasible sets, CDO constitutes a more relevant baseline for evaluating the effectiveness of AO and JO in the present problem. The effectiveness of these methods is evaluated from four complementary aspects: achievable sum-rate performance, statistical performance distribution, convergence behavior under different feasible initializations, and computation-time comparison.

Figure 2 illustrates the achievable sum rate of JO, AO, and the CDO benchmark versus the nominal transmit-side SNR. As the SNR increases, the sum rate of all three methods improves monotonically, since a higher transmit power enhances the effective communication link. Among the compared methods, JO consistently achieves the highest sum rate over the entire tested SNR range, while AO remains the second-best method and maintains a clear performance advantage over the CDO benchmark. In addition, the growth of all three curves becomes less pronounced in the medium-to-high SNR region, indicating a gradual saturation trend. Overall, these results show that both JO and AO are effective

structured optimization approaches under the considered constant-modulus constraints, with JO providing the best achievable sum-rate performance in the present setting.

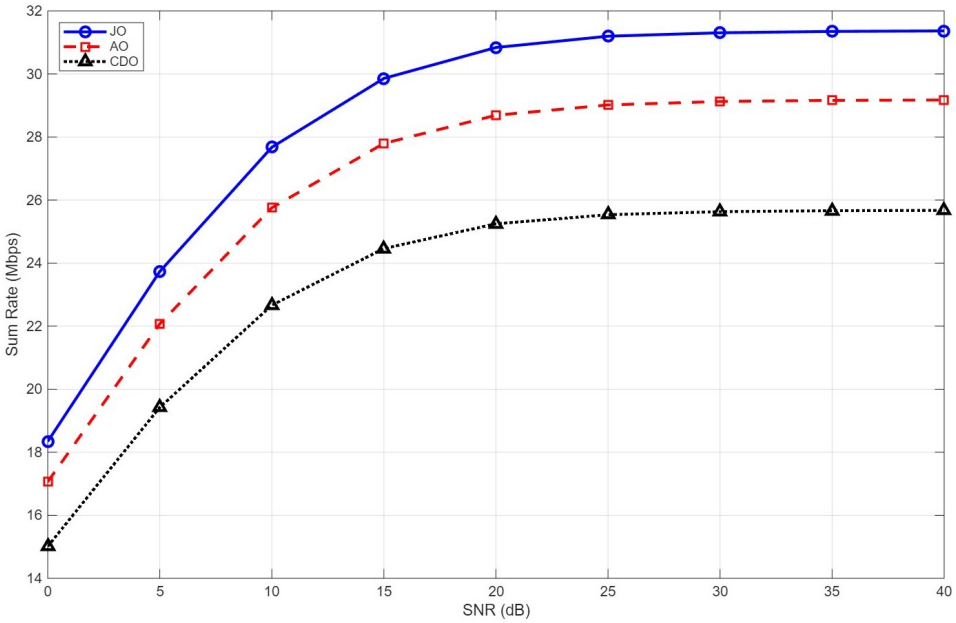



**Figure 2.** Achievable sum rate versus nominal transmit-side SNR for JO, AO and CDO.

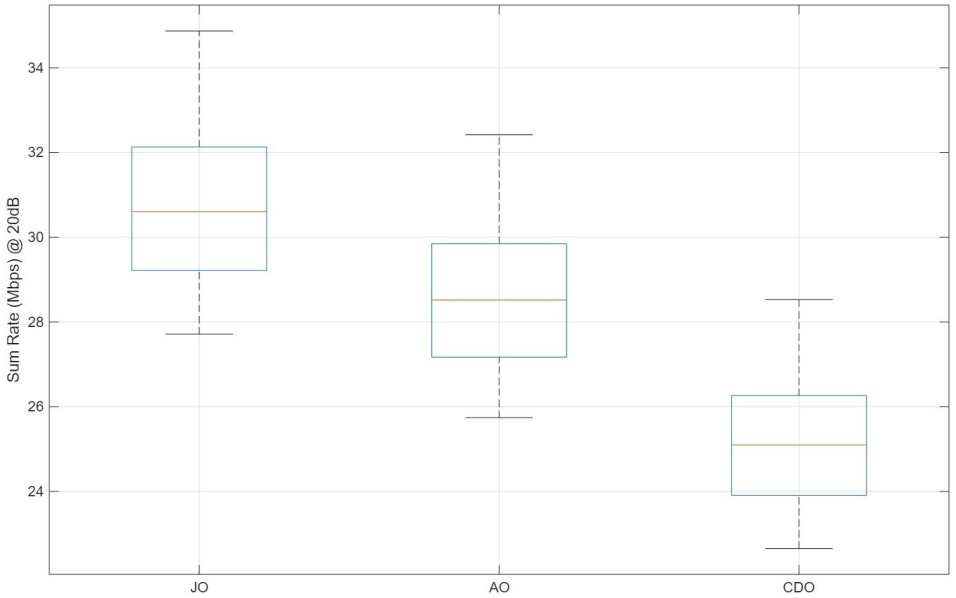



**Figure 3.** Boxplot of achievable sum rate over independent Monte Carlo trials for JO, AO and CDO.

Figure 3 provides a statistical comparison of the achievable sum rate obtained by JO, AO, and CDO at SNR = 20 dB. The boxplot shows that JO attains the highest median sum rate and also occupies the highest overall performance region among the three methods. AO ranks second, with its distribution clearly below that of JO but still noticeably above the CDO benchmark. In contrast, CDO is centered at a substantially lower rate level, indicating an evident performance disadvantage under the same simulation setting. Moreover, the distributional separation among the three methods suggests that the advantage of JO is not due to only a few favorable samples, but is reflected in the overall sample statistics as well.

Figure 4 compares the convergence trajectories of JO, AO, and CDO at SNR = 20 dB under SVD-based initialization. It can be observed that all three methods improve rapidly

during the initial iterations and then gradually approach stable solutions. Among them, JO maintains the highest sum-rate level throughout almost the entire iteration process and reaches the highest stable performance. AO also exhibits faster empirical convergence, but its stable rate remains below that of JO. In contrast, CDO stays consistently lower than both JO and AO over the whole iteration range. In addition, mild fluctuations can be observed before the curves fully stabilize, which is typical in iterative non-convex optimization. Overall, these results indicate that under SVD-based initialization at 20 dB, JO achieves the best convergence trajectory and the highest final sum-rate performance, while AO remains competitive and CDO is clearly inferior.

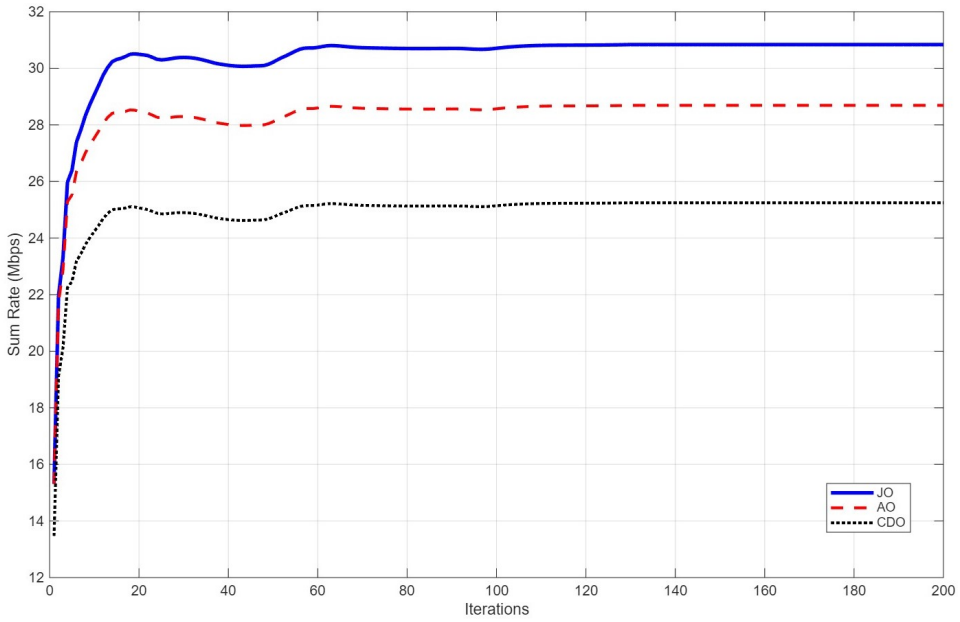



**Figure 4.** Convergence comparison of JO, AO and CDO under SVD-phase initialization.

Figure 5 shows the convergence trajectories of JO, AO, and CDO at SNR = 20 dB under random feasible initialization. Compared with the SVD-based initialization case in Figure 4, the overall convergence becomes slightly slower and the early-stage fluctuations are more visible, indicating a higher sensitivity to the initialization quality. Nevertheless, all three methods still exhibit stable empirical convergence behavior after sufficient iterations. In terms of final performance, JO remains the best-performing method, AO reaches the second-highest stable rate, and CDO stays at the lowest level. Therefore, although random feasible initialization degrades the convergence behavior to some extent relative to SVD-based initialization, it does not change the overall performance ranking among the three methods.

Table 3 reports the measured computation time of JO, AO, and CDO under SVD-based and random feasible initializations. In both initialization settings, JO shows the highest runtime, AO requires the least runtime, and CDO remains between the two. Moreover, random initialization consistently results in longer runtime than SVD-based initialization for all three methods. This suggests that initialization quality affects the practical computational efficiency in addition to the iteration-level convergence behavior. Overall, these empirical timing results are in line with the discussion in Section 3.3, where the computational comparison is understood to depend on both asymptotic complexity characteristics and practical factors such as iteration count and initialization sensitivity.

**Table 3.** Computation time comparison of JO, AO, and CDO under different initializations

| Initialization | JO (s) | AO (s) | CDO (s) |
|---|---|---|---|
| SVD | 2.9273 | 0.0105 | 0.0602 |
| Random | 4.2412 | 0.0177 | 0.0713 |

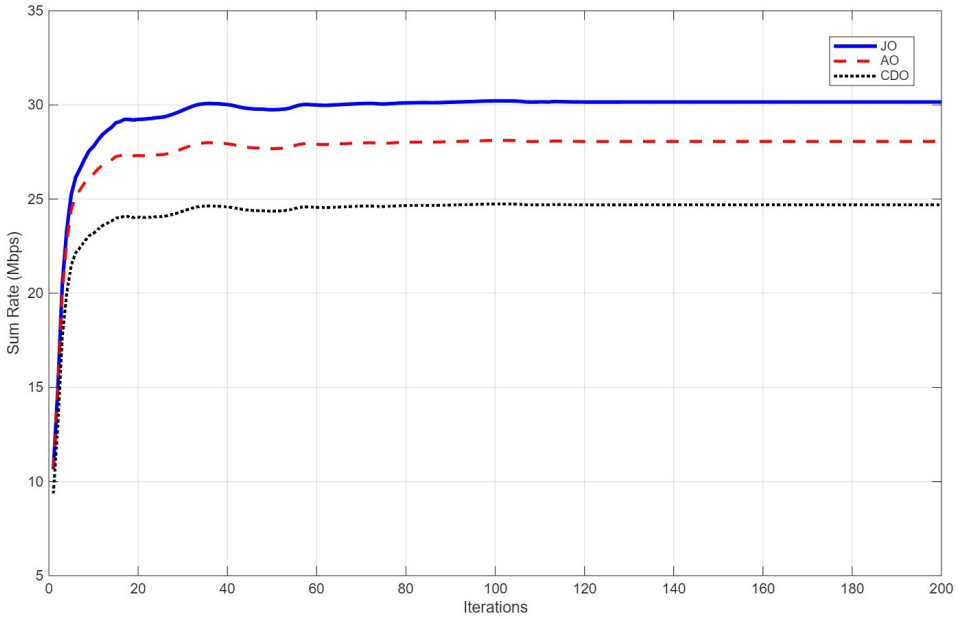



**Figure 5.** Convergence comparison of JO, AO and CDO under random feasible initialization.

Taken together, the above results also help clarify the practical advantages and limitations of the proposed methods.

Compared with the CDO benchmark, both proposed methods achieve clear performance gains under the same constant-modulus transceiver constraints. In particular, JO attains the highest achievable sum-rate performance, while AO also consistently outperforms CDO, which confirms the effectiveness of the proposed optimization frameworks for the considered hardware-constrained beamforming problem. Meanwhile, the two methods exhibit different practical tradeoffs. JO is more favorable in terms of final performance, but its limitation is the higher runtime required to achieve such performance. By contrast, AO is more attractive in terms of runtime and computational efficiency, but its limitation is that the final achievable sum-rate level is generally lower than that of JO. Therefore, the proposed methods should be viewed as two complementary solution choices rather than uniformly superior solutions, with JO being more suitable for performance-oriented settings and AO being more suitable for computation-constrained implementations.

## 5. Conclusions

This paper investigated the joint beamforming optimization problem for narrowband IoV backhaul under constant-modulus constraints. To address the non-convexity arising from this formulation, two structured numerical frameworks, namely AO and JO, were developed. Simulation results showed that both methods can significantly improve the achievable sum rate compared with the CDO benchmark. Meanwhile, the complexity analysis and numerical results also revealed that AO and JO exhibit different computational and convergence characteristics. Specifically, AO exhibits faster empirical convergence and lower measured runtime, whereas JO requires more iterations but achieves better final sum-rate performance. In addition, the comparison under different initialization strategies shows that SVD-based initialization provides a more structured starting point and generally

leads to better empirical convergence behavior and lower runtime than random feasible initialization. These findings suggest that the practical comparison between AO and JO should not be based solely on the final achievable performance, but should also take into account convergence speed, initialization sensitivity, and empirical computational efficiency. Future work will focus on improving the empirical convergence behavior of AO, reducing the initialization sensitivity and runtime of JO, and extending the current framework to more realistic wideband and time-varying IoV channel scenarios. These results provide a valuable computational reference for the deployment of high-capacity and reliable wireless backhaul solutions in future intelligent transportation systems.

**Author Contributions:** Conceptualization, H.Z.; software, Z.W.; formal analysis, H.Z.; investigation, Z.W.; resources, C.Z.; data curation, C.Z.; writing—original draft, H.Z.; writing—review and editing, H.T.; visualization, X.H. All authors have read and agreed to the published version of the manuscript.

**Funding:** This research did not receive external fundings.

**Data Availability Statement:** The original contributions presented in this study are included in the article. For further inquiries, please contact the corresponding author.

**Conflicts of Interest:** The authors declare no conflicts of interest.

## References

1. Hartenstein, H.; Laberteaux, K. A tutorial survey on vehicular ad hoc networks. *IEEE Commun. Mag.* **2008**, *46*, 164–171. [CrossRef]
2. Mecklenbräuker, C.F.; Molisch, A.F.; Karedal, J.; Tufvesson, F.; Paier, A.; Bernado, L. Vehicular channel characterization and its implications for wireless system design and performance. *Proc. IEEE* **2011**, *99*, 1189–1212. [CrossRef]
3. Goldsmith, A. *Wireless Communications*; Cambridge University Press: Cambridge, UK, 2005.
4. Clerckx, B.; Oestges, C. *MIMO Wireless Networks: Channels, Techniques and Standards for Multi-Antenna, Multi-User and Multi-Cell Systems*; Academic Press: Cambridge, MA, USA, 2013.
5. Molisch, A.F.; Ratnam, V.V.; Han, S.; Li, Z.; Nguyen, S.-L.H.; Li, L.; Haneda, K. Hybrid beamforming for massive MIMO: A survey. *IEEE Commun. Mag.* **2017**, *55*, 134–141. [CrossRef]
6. Ioushua, S.S.; Eldar, Y.C. A family of hybrid analog–digital beamforming methods for massive MIMO systems. *IEEE Trans. Signal Process.* **2019**, *67*, 3243–3261. [CrossRef]
7. Luo, Z.-Q.; Ma, W.-K.; So, A.M.-C.; Ye, Y.; Zhang, S. Semidefinite relaxation of quadratic optimization problems. *IEEE Signal Process. Mag.* **2010**, *27*, 20–34. [CrossRef]
8. Ibrahim, L.; Mahmud, M.N.; Salleh, M.F.M.; Muhammad, S.I.; Yusof, S.K.S. Joint beamforming optimization design and performance evaluation of RIS-aided wireless networks: A comprehensive state-of-the-art review. *IEEE Access* **2023**, *11*, 141801–141859. [CrossRef]
9. Arora, A.; Tsinos, C.G.; Bhavani Shankar, M.R.; Chatzinotas, S.; Ottersten, B. Efficient algorithms for constant-modulus analog beamforming. *IEEE Trans. Signal Process.* **2022**, *70*, 756–771. [CrossRef]
10. Nguyen, N.; Xie, L.; Chen, D.; Cao, M.; Hanzo, L. Deep unfolding hybrid beamforming designs for THz massive MIMO systems. *IEEE Trans. Signal Process.* **2023**, *71*, 3788–3804. [CrossRef]
11. Luo, H.; Liu, R.; Li, M.; Liu, Y.; Liu, Q. Joint beamforming design for RIS-assisted integrated sensing and communication systems. *IEEE Trans. Veh. Technol.* **2022**, *71*, 13393–13397. [CrossRef]
12. Griffiths, L.; Jim, C.W. An alternative approach to linearly constrained adaptive beamforming. *IEEE Trans. Antennas Propag.* **1982**, *30*, 27–34. [CrossRef]
13. Rusek, F.; Persson, D.; Lau, B.K.; Larsson, E.G.; Marzetta, T.; Edfors, O.; Tufvesson, F. Scaling up MIMO: Opportunities and challenges with very large arrays. *IEEE Signal Process. Mag.* **2013**, *30*, 40–60. [CrossRef]
14. Heath, R.W.; González-Prelcic, N.; Rangan, S.; Rappaport, T.S.; Samimi, M. An overview of signal processing techniques for millimeter wave MIMO systems. *IEEE J. Sel. Top. Signal Process.* **2016**, *10*, 436–453. [CrossRef]
15. He, S.; Du, J.; Liao, Y. Multi-User Scheduling for 6G V2X Ultra-Massive MIMO System. *Sensors* **2021**, *21*, 6742. [CrossRef]
16. Li, S.; Li, C.; Tan, W.; Ji, B.; Yang, L. Robust Beamforming Design for Secure V2X Downlink System with Wireless Information and Power Transfer under a Nonlinear Energy Harvesting Model. *Sensors* **2018**, *18*, 3294. [CrossRef]
17. Xie, J.; Tian, C.; Xu, Z.; He, C.; Zhao, Y. An Energy-Efficient Resource Allocation Strategy in Massive MIMO-Enabled Vehicular Edge Computing Networks. *High-Confid. Comput.* **2023**, *3*, 100130. [CrossRef]

18. Mohammed, S.K.; Larsson, E.G. Per-antenna constant envelope precoding for large multi-user MIMO systems. *IEEE Trans. Commun.* **2013**, *61*, 1059–1071. [CrossRef]
19. Chen, J.-C.; Wen, C.-K.; Wong, K.-K. Improved constant envelope multiuser precoding for massive MIMO systems. *IEEE Commun. Lett.* **2014**, *18*, 1311–1314. [CrossRef]
20. Shi, S.; Cai, Y.; Hu, Q.; Champagne, B.; Hanzo, L. Deep-unfolding neural-network aided hybrid beamforming based on symbol-error probability minimization. *IEEE Trans. Veh. Technol.* **2023**, *72*, 529–545. [CrossRef]
21. Zhu, X.; Wang, L.; Huang, C.; Yang, Z.; Chen, X.; Al Hammadi, A. Robust beamforming for RIS-aided communications via gradient-based manifold meta learning. *IEEE Trans. Wireless Commun.* **2024**, *23*, 15945–15956. [CrossRef]
22. Zhong, K.; Hu, J.; Li, H.; Wang, R.; An, D.; Zhu, G.; Teh, K.C.; Pan, C.; Eldar, Y.C. RIS-Aided Beamforming Design for MIMO Systems via Unified Manifold Optimization. *IEEE Trans. Veh. Technol.* **2025**, *74*, 674–685. [CrossRef]
23. Soltanalian, M.; Stoica, P. Designing unimodular codes via quadratic optimization. *IEEE Trans. Signal Process.* **2014**, *62*, 1221–1234. [CrossRef]
24. Shi, Q.; Razaviyayn, M.; Luo, Z.-Q.; He, C. An iteratively weighted MMSE approach to distributed sum-utility maximization for a MIMO interfering broadcast channel. *IEEE Trans. Signal Process.* **2011**, *59*, 4331–4340. [CrossRef]
25. Razaviyayn, M.; Hong, M.; Luo, Z.-Q. A unified convergence analysis of block successive minimization methods for nonsmooth optimization. *SIAM J. Optim.* **2013**, *23*, 1126–1153. [CrossRef]
26. Nocedal, J.; Wright, S.J. *Numerical Optimization*, 2nd ed.; Springer: New York, NY, USA, 2006.
27. Vu, T.T.; Raviv, Y.; Raich, R.; Xiao, F. On local linear convergence of projected gradient descent for unit-modulus least squares. *IEEE Trans. Signal Process.* **2023**, *71*, 3883–3897. [CrossRef]
28. Absil, P.-A.; Mahony, R.; Sepulchre, R. *Optimization Algorithms on Matrix Manifolds*; Princeton University Press: Princeton, NJ, USA, 2008.
29. Saleh, A.A.M.; Valenzuela, R.A. A statistical model for indoor multipath propagation. *IEEE J. Sel. Areas Commun.* **1987**, *5*, 128–137. [CrossRef]
30. Ugray, Z.; Lasdon, L.; Plummer, J.; Glover, F.; Kelly, J.; Martí, R. Scatter search and local NLP solvers: A multistart framework for global optimization. *INFORMS J. Comput.* **2007**, *19*, 328–340. [CrossRef]


**Disclaimer/Publisher's Note:** The statements, opinions and data contained in all publications are solely those of the individual author(s) and contributor(s) and not of MDPI and/or the editor(s). MDPI and/or the editor(s) disclaim responsibility for any injury to people or property resulting from any ideas, methods, instructions or products referred to in the content.